Chalcogenide Letters Vol. 22, No. 11, November 2025, p. 939 - 949

Emitter/Absorber Interface Design Strategies for Se Solar Cells

Fan He[1,2,3,*], Xu He[4], Jie Wang[1] and Yu Hu[5]

[1]School of Physics and Astronomy, China West Normal University, Nanchong, 637200, China
[2]Chengdu Institute of Computer Application, Chinese Academy of Sciences, Chengdu, 610041, China
[3]Leshan Vocational and Technical College, Leshan, 614000, China
[4]Chengdu Textile College, Chengdu, 611731, China
[5]Leshan West Silicon Materials Photovoltaic New Energy Industry Technology Research Institute, Leshan, 614000, China
*Corresponding Author: F. He. Email: hefan@cwnu.edu.cn

Received: 17 July 2025; Accepted: 6 November 2025

ABSTRACT: Selenium (Se) has garnered significant attention as a promising wide-bandgap material for photovoltaic applications. However, progress in enhancing the efficiency of Se solar cells remains limited. This study addresses this challenge by targeting the critical emitter/Se absorber interface for performance improvement. Through numerical simulations, we systematically investigate the impact of key interface properties—specifically, band alignment and defect characteristics—on device performance. Our results demonstrate that a slight positive conduction band offset (CBO) effectively strengthens absorber band bending and reduces hole concentration at the Se surface. Furthermore, minimizing interface defect density or incorporating donor-type defects significantly alleviates interfacial recombination. Building on these findings, we propose a novel interface passivation strategy employing an ultra-thin dielectric layer engineered with positive fixed charges or hydrogen atoms. This approach is anticipated to substantially suppress recombination losses and enhance the performance of Se solar cells, facilitating their broader adoption in photovoltaics.

KEYWORDS: Se solar cells; numerical simulation; band alignment; interface defects; interface passivation

---

1 Introduction

Selenium (Se) has regained significant attention as an established candidate material for wide-bandgap photovoltaic applications. The tunable bandgap of trigonal Se thin films, ranging typically from 1.77 to 1.95 eV [1–5] depending on preparation conditions, positions them ideally as top-cell absorbers in tandem solar cell architectures [6–9]. This suitability is further enhanced by Se's low melting point (~220°C), which facilitates thin-film preparation and annealing while maintaining compatibility with bottom-cell processing in stacked configurations. The inherent wide bandgap also contributes to a relatively high open-circuit voltage (V_{oc}), with reported values exceeding 900 mV [3,6,10]. Moreover, as a direct bandgap semiconductor, Se exhibits a high absorption coefficient ($>10^5$ cm^{-1}) within the relevant solar spectrum. This combination of properties is exemplified by early demonstrations, such as Todorov et al.'s achievement [2] of 2.7% efficiency using only a 20-nm-thick Se absorber. Consequently, Se solar cells hold considerable promise for specialized applications including wearable electronics, flexible devices, building-integrated photovoltaics (BIPV), and indoor photovoltaics (IPVs) [11–13].

Driven by increasing interest in wide-bandgap photovoltaics, research on Se solar cells has advanced substantially over the past decade. Building on foundational work, Todorov et al. [2] set a significant milestone by employing $Zn_xMg_{1-x}O$ (MZO) as the electron transport layer (ETL) and MoO_x as the hole transport layer (HTL), achieving a certified efficiency of 6.5%. More recent breakthroughs came from Xue et al., who developed a critical melting–annealing (CMA) strategy. This technique integrates disordered one-dimensional Se chains into the trigonal lattice, enabling Se cells to reach efficiencies of 7.2% under standard AM 1.5 G illumination and 18.0% under 1000-lux indoor lighting [14]. Further optimization through substrate-heating, promoting vertical Se film growth, pushed the AM 1.5 G efficiency to 8.1%

https://doi.org/10.15251/CL.2025.2211.939

[15]. Notably, Xue's group also introduced a molten Se glue-bonding strategy, achieving a state-of-the-art efficiency of 8.61% under 1-sun illumination [16].

Notwithstanding these advances, significant performance limitations persist. The current record efficiency represents only ~32.9% of the Shockley-Queisser theoretical limit for Se [3], indicating substantial potential for improvement and the existence of critical loss mechanisms. Enhancing Se solar cell performance remains challenging, demanding focused efforts on mitigating these losses.

The emitter/absorber interface critically governs device performance by controlling the built-in electric field and photogenerated carrier separation. To achieve further efficiency gains in Se solar cells, deeper understanding of interface properties and advanced engineering strategies are essential. In this work, we therefore systematically investigate—through numerical simulations—the impact of key interfacial characteristics (band alignment and defect properties) on device performance. These insights establish design principles for interface optimization and enable a novel passivation strategy to suppress recombination and enhance efficiency.

2 Device Structures and Analysis

The simulations employed the established one-dimensional solar cell simulation software SCAPS-1D, developed by the Department of Electronics and Information Systems (ELIS) at the University of Ghent, Belgium. While initially designed for $CuInSe_2$ and CdTe-based solar cells, SCAPS-1D has been extended through recent advancements to simulate various heterojunction polycrystalline thin-film devices [17–19]. Focusing on the emitter/Se interface, we simulated a simplified device structure (see Fig. 1) consisting of a front contact, a 60-nm-thick electron transport layer (ETL), a 400-nm-thick Se absorber layer, and a back contact. The front contact metal work function was set to 3.9 eV with a surface reflectivity of 8%. To systematically study the conduction band offset (CBO) at the ETL/Se interface, the electron affinity (χ) of the ETL was varied between 3.3 and 4.4 eV, while that of the Se absorber was fixed at 3.8 eV. The CBO, defined as $\chi_{ETL} - \chi_{Se}$, thus ranged from −0.5 eV ("cliff") to +0.6 eV ("spike"). The bulk carrier lifetime in Se was fixed at 1 ns, and the shallow acceptor density (hole density, p_{Se}) was systematically varied to assess its impact alongside interface characteristics. An ohmic back contact (simulated as a flat band condition) was assumed. Additional fundamental material parameters used in the simulations (Table 1) were adopted from the literatures [3,4,6,18].

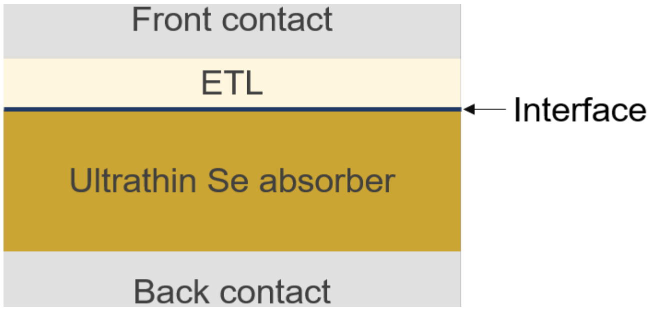

Figure 1: Simplified Se solar cell structure used for SCAPS simulation.

Table 1: Parameters for numerical simulation discussed in this work.

Device parameters		
	Front contact	Back contact
Φ_m (eV)	3.9	Flat band
S_e (cm/s)	10^7	10^7
S_h (cm/s)	10^7	10^7
Layer properties		
	ETL	Se
W (nm)	60	400

$\varepsilon/\varepsilon_0$	10	9.4
μ_e (cm^2/V·s)	100	15
μ_h (cm^2/V·s)	25	3
V_e (cm/s)	1×10^7	1×10^7
V_h (cm/s)	1×10^7	1×10^7
n/p (cm^{-3})	10^{18}	10^{13}–10^{16}
E_g (eV)	3.2	1.84
N_c (cm^{-3})	2.2×10^{18}	8×10^{17}
N_v (cm^{-3})	1.8×10^{19}	1.8×10^{19}
χ (eV)	3.3–4.4	3.8
Single (midgap) defect states		
	ETL	Se
$N_{t,D}/N_{t,A}$ (cm^{-3})	A: 8×10^{17}	D: 10^{13}
σ_e (cm^2)	10^{-17}	10^{-11}
σ_h (cm^2)	10^{-12}	10^{-14}

Note: The work function of electrode Φ_m, surface recombination velocity S_e/S_h, relative dielectric constant $\varepsilon/\varepsilon_0$, film thickness W, mobility μ_e/μ_h, carrier density n/p, band gap E_g, density of states N_c/N_v, electron affinity χ, the donor-type/acceptor-type defect density $N_{t,D}/N_{t,A}$, capture cross section σ_e/σ_h.

3 Results and Discussions

3.1 The Emitter/Absorber Band Alignment

First, we examined the effect of the emitter/absorber band alignment, characterized by the conduction band offset (CBO), on the performance of Se solar cells. Fig. 2 shows the simulated *J-V* characteristics for 400-nm-thick Se solar cells under varying CBOs. In these simulations, key parameters were fixed: the hole concentration in Se at 2×10^{14} cm^{-3}, the ETL/Se interface defect type as mid-gap acceptor states, and the interfacial recombination velocity (S_{IF}) at 5×10^4 cm/s. The results demonstrate a pronounced enhancement in device performance with increasing CBO. However, excessively large CBO values induce an S-shaped kink in the *J-V* curve, substantially reducing the fill factor (FF).

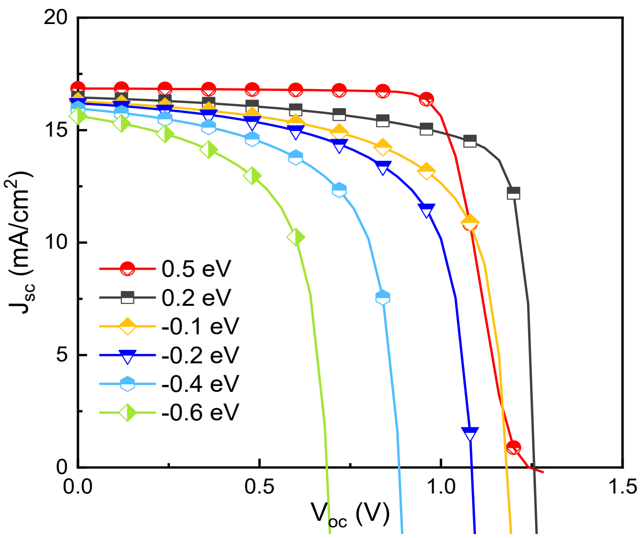

Figure 2: J-V characteristics of 400 nm Se solar cells as a function of CBOs. Simulations employed a bulk carrier lifetime of 1 ns, a Se hole concentration of 2×10^{14} cm^{-3}, an interface recombination velocity of 5×10^4 cm s^{-1}, and mid-gap acceptor-type defect states.

To elucidate the underlying mechanisms behind the performance trends observed in Fig. 2, Fig. 3 present the band diagrams, electric field distributions, and carrier concentration profiles for Se solar cells with CBOs of +0.2 and −0.2 eV. A representative bias voltage of +0.9 V, within the operational range, was applied to highlight band bending effects. The band diagram in Fig. 3a reveals that a CBO of +0.2 eV creates a modest electron barrier at the interface. Crucially, as demonstrated in Fig. 2, this barrier does not impede electron transport; instead, it enhances device performance. This enhancement arises because the positive CBO intensifies band bending and increases the built-in potential, forming a conduction band spike. Furthermore, Fig. 3a shows that with a +0.2 eV CBO, the conduction band minimum (E_c) of Se lies closer to the electron Fermi level (E_{fn}), while the valence band maximum (E_v) is farther from the hole Fermi level (E_{fp}). This alignment indicates a more pronounced inversion layer and a reduced minority carrier (hole) concentration at the Se surface, thereby decreasing recombination current. Conversely, the band diagram for a −0.2 eV CBO (Fig. 3d) shows relatively weak band bending at the interface, suggesting weaker inversion. This configuration allows for greater hole recombination at the surface, explaining the lower output voltage observed with negative CBOs.

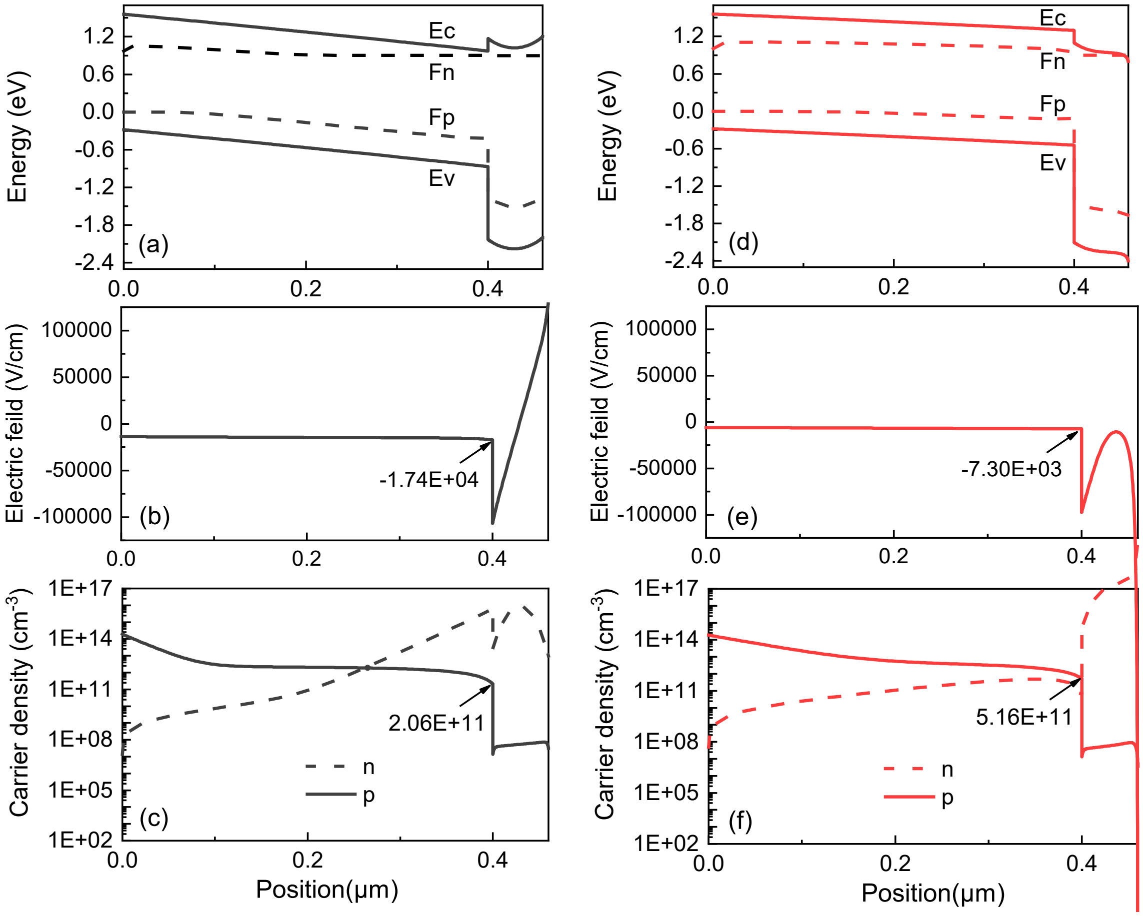

Figure 3: (**a**,**d**) Band diagrams, (**b**,**e**) electric field distribution diagrams and (**c**,**f**) carrier density profiles for Se solar cells with CBO of +0.2 and −0.2 eV, respectively, at 0.9 V bias voltage. Note that the illumination is applied on the right side.

Further insights into interfacial recombination, which is fundamentally governed by defects, can be gained from interface physics and the Shockley-Read-Hall (SRH) recombination model. The interfacial recombination rate (R_{IF}) is analytically expressed as follows [20,21]:

$$R_{IF} = \frac{n_{IF}p_{IF} - n_i^2}{S_p^{-1}\left(n_{IF} + n^*\right) + S_n^{-1}\left(p_{IF} + p^*\right)} \tag{1}$$

In the equation, n_{IF} and p_{IF} denote the electron and hole concentrations at the interface, respectively, while n_i is the intrinsic carrier concentration. S_n and S_p represent the interfacial recombination velocities for electrons and holes, respectively. The variables n* and p* represent the densities of defect electrons and defect holes, respectively, which account for the generation of free electrons and holes from the defect states.

For small injections, the interfacial recombination rate of a n-type surface (an n-type inversion layer is formed near the front interface of the Se absorption layer) can be simplified as follows [20]:

$$R_{IF} = S_{IF} \times p_{IF,a} \tag{2}$$

It is evident that the R_{IF} is governed by the interfacial recombination velocity and minority (hole) carrier concentration at the Se surface.

Concurrently, the open-circuit voltage of the solar cell can be formulated as shown in Eq. (3), derived from the diode's output characteristics under illumination.

$$V_{oc} = \frac{kT}{q}\ln\left(\frac{J_L}{J_0} + 1\right) \tag{3}$$

Eq. (3) suggests that the V_{oc} of the cell is predominantly influenced by the photogenerated current density (J_L) and the saturation current density (J_0). J_0 is highly sensitive to recombination processes, thus excessive recombination (high J_0 value) can severely degrade the V_{oc}. This is a primary factor contributing to the lower V_{oc} observed in Se solar cells.

The enhanced performance of Se solar cells under positive CBO, as revealed by the band diagrams in Fig. 3a,d, is further elucidated by the associated electric field and carrier distributions. Specifically, the stronger electric field observed in the cell with a +0.2 eV CBO (Fig. 3b) compared to the −0.2 eV case (Fig. 3e) facilitates the collection of photogenerated charge carriers. Furthermore, the simulated carrier density profiles (Fig. 3c,f) confirm a reduced concentration of holes (minority carriers) at the Se surface under positive CBO alignment. This reduction in minority carrier density at the interface is consistent with the band diagram analysis and implies a lower interfacial recombination rate. Consequently, as demonstrated in Fig. 4, the recombination current density is significantly reduced across different bias voltages for the cell featuring a +0.2 eV CBO relative to its counterpart with a −0.2 eV CBO.

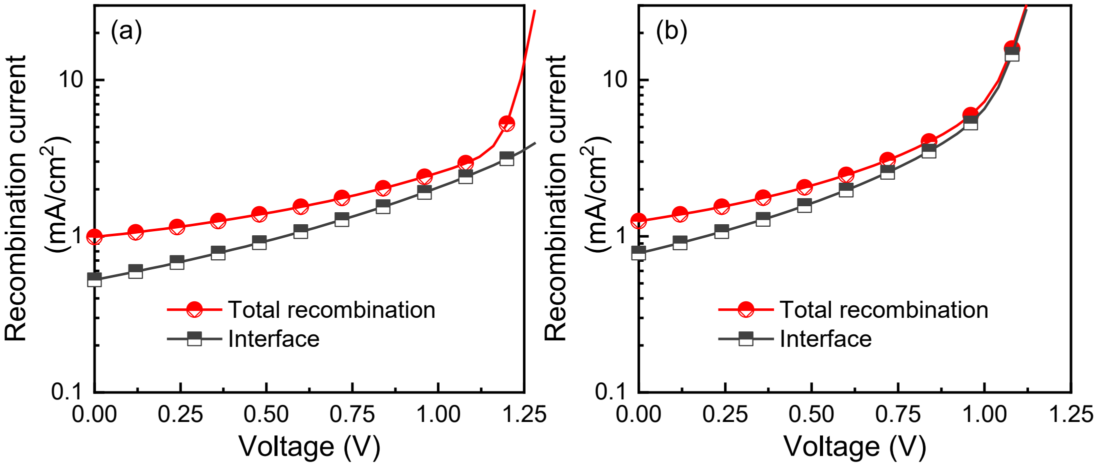

Figure 4: Recombination current densities as a function of bias voltage when CBO is (**a**) +0.2 and (**b**) −0.2 eV.

The preceding discussion demonstrates the critical role of the CBO at the emitter/Se absorber interface in determining both current collection and open-circuit voltage in Se solar cells. A positive CBO effectively mitigates interfacial recombination by enhancing band bending and suppressing minority carrier recombination. Consequently, selecting ETL materials that yield a small conduction band spike is a key strategy for achieving high-performance Se devices. However, the inherent low electron affinity of Se (~3.8 eV) typically results in a conduction band cliff when paired with common ETLs such as CdS, ZnO, TiO_2, and SnO_2 [22,23]. This unfavorable band alignment represents a significant constraint on Se solar cell development. $Mg_xZn_{1-x}O$ (MZO) emerges as a promising alternative ETL candidate due to its relatively low and composition-tunable electron affinity (via Mg content adjustment). The use of MZO in the previous record-efficiency Se cell [2] supports this potential. Nevertheless, a substantial conduction band cliff persists even between Se and reported MZO compositions, highlighting an unresolved challenge. Further research is therefore essential to discover superior ETL materials capable of realizing an optimal band alignment with minimal cliff.

3.2 Interface Defects

In heterojunction devices, interface defect states arise from lattice mismatch and dangling bonds, which can perturb band bending. In the simulations presented above, interface defects were modeled exclusively as acceptor-type states. Upon capturing electrons, these acceptor-defects become negatively charged. This negative charge reduces the electron concentration at the interface and diminishes band bending within the absorber layer, thereby degrading the band alignment of the solar cell, as illustrated in Fig. 5a. Conversely, donor-type interface defects introduce positive charges upon ionization. These positive charges decrease the hole concentration at the Se surface, enhancing band bending in the absorber (Fig. 5b) and consequently alleviating interfacial recombination.

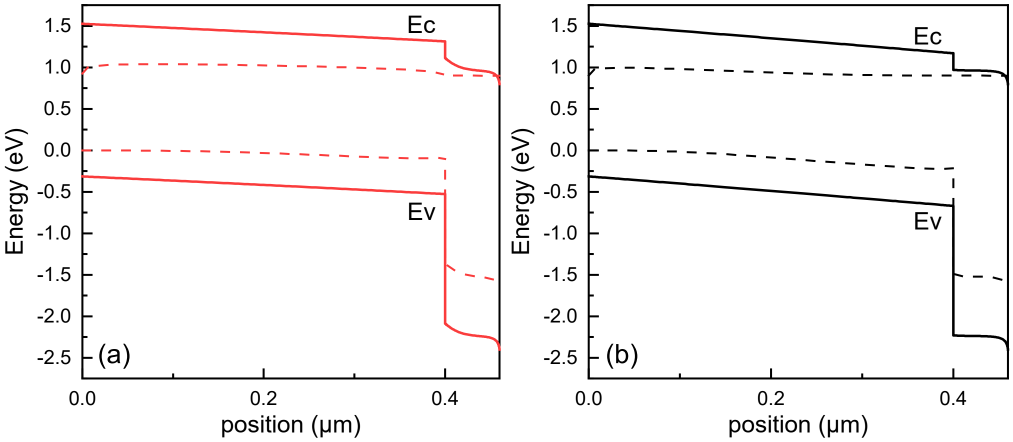

Figure 5: Band diagrams for Se solar cells of (**a**) acceptor and (**b**) donor-type interface defects at 0.9 V bias voltage with CBO of −0.2 eV. Note that the illumination is applied on the right side.

Fig. 6 presents the performance of Se solar cells for both acceptor- and donor-type interface defects under two distinct CBO conditions. The results demonstrate that donor-type defects enhance device performance regardless of the CBO sign. Specifically, in the presence of a conduction band cliff (negative CBO), which exacerbates interface recombination, donor-type defects exert a more pronounced positive impact on V_{oc}. Conversely, when a modest conduction band spike (positive CBO) exists, donor-type defects do not substantially reduce interface recombination. In this case, the performance improvement primarily stems from an increase in FF. These findings collectively indicate that implementing a small conduction band spike design mitigates the influence of interface defect states on overall device performance.

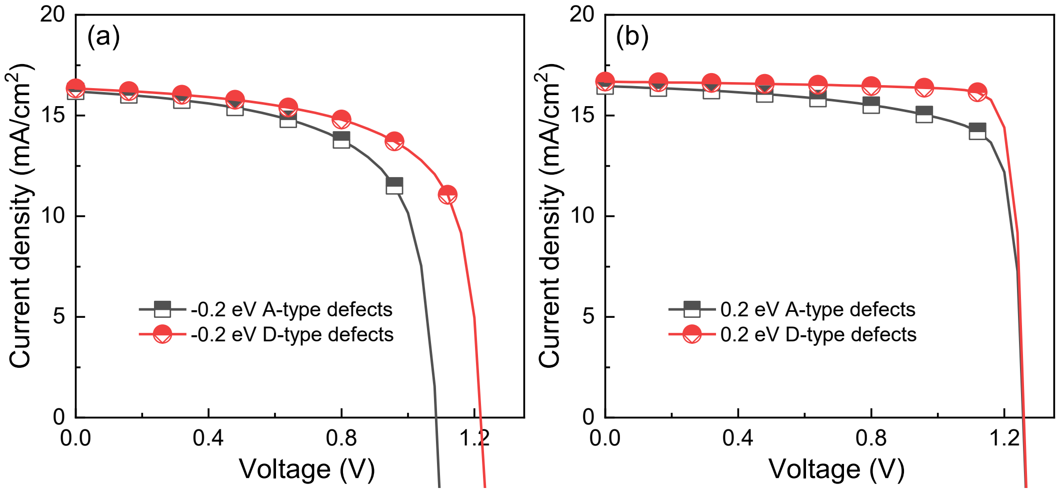

Figure 6: J-V characteristics for the 400 nm thick Se solar cells of acceptor (A) and donor (D) type-interface defects with CBO of (**a**) −0.2 and (**b**) +0.2 eV. The carrier lifetime was maintained at 1 ns, p_{Se} was 2×10^{14} cm^{-3}, and S_{IF} was 5×10^4 cm/s.

Fig. 7 comprehensively analyzes the combined effects of interface defect type, conduction band offset, and interface recombination velocity (S_{IF}) on device efficiency. As expected, lower S_{IF} values generally yield superior cell performance. When S_{IF} is reduced to 1×10^2 cm/s, Se cell efficiency reaches ~19%, independent of defect type (acceptor or donor). Crucially, optimal interface design (appropriate CBO and defect type) can attenuate the detrimental effects of high S_{IF}. For example, with donor-type defects and a +0.2 eV CBO, efficiencies exceeding 17% are maintained even at $S_{IF} = 1 \times 10^5$ cm/s. This resilience arises because interfacial recombination is suppressed by the scarcity of holes available for recombination with electrons at the interface. Consequently, efficiency becomes markedly less sensitive to interface defect density (which governs S_{IF}).

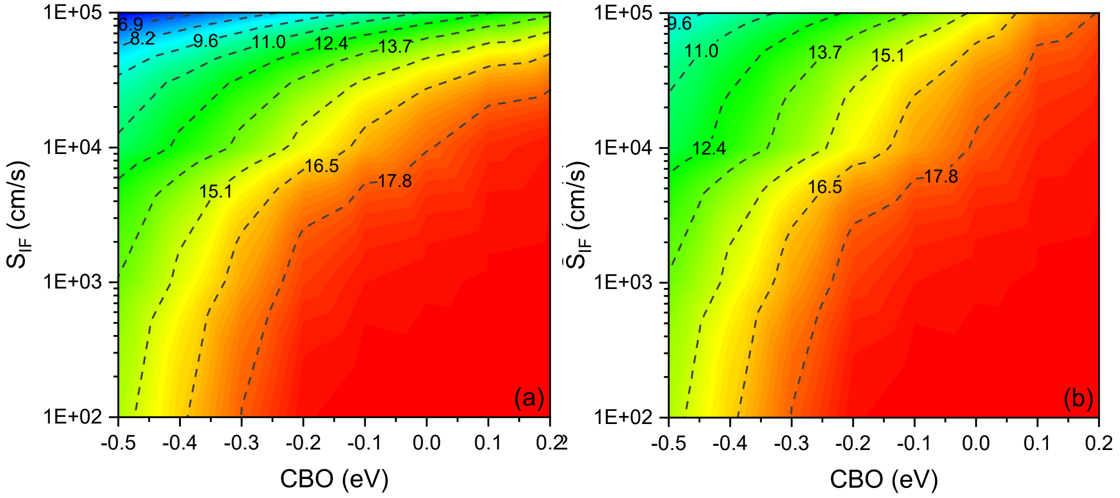

Figure 7: Contour plots of the efficiency for Se solar cells as a function of S_{IF} and CBO, and varying interface defect types: (**a**) Acceptor-type interface defects; (**b**) Donor-type interface defects.

These results demonstrate that interfacial recombination is governed by two factors: interfacial recombination velocity (S_{IF}) and minority carrier concentration at the absorber surface. Elevated minority carrier concentration—occurring with negative CBO or acceptor-type defects—demands lower S_{IF} (i.e., reduced defect density) to effectively suppress recombination. Conversely, strong surface inversion—induced by positive CBO or donor-type defects—renders device performance largely independent of S_{IF}.

While doping enhances the built-in electric field and has been shown to improve V_{oc} in Se solar cells, its effectiveness is constrained by interface quality. The theoretical relationship between carrier concentration and built-in potential is described by:

$$V_{\text{built-in}} = \frac{kT}{q} \ln\left(\frac{N_A N_D}{n_i^2}\right) \tag{4}$$

However, our simulations reveal a critical interface-dependent limitation. Fig. 8 demonstrates that increasing hole concentration degrades V_{oc} in devices with severe interfacial recombination (high S_{IF} or acceptor-type defects). This counterintuitive effect stems from amplified recombination currents at interfaces. Consequently, interfacial recombination fundamentally constrains doping strategies for V_{oc} enhancement, necessitating co-optimization of interface passivation and bulk doping.

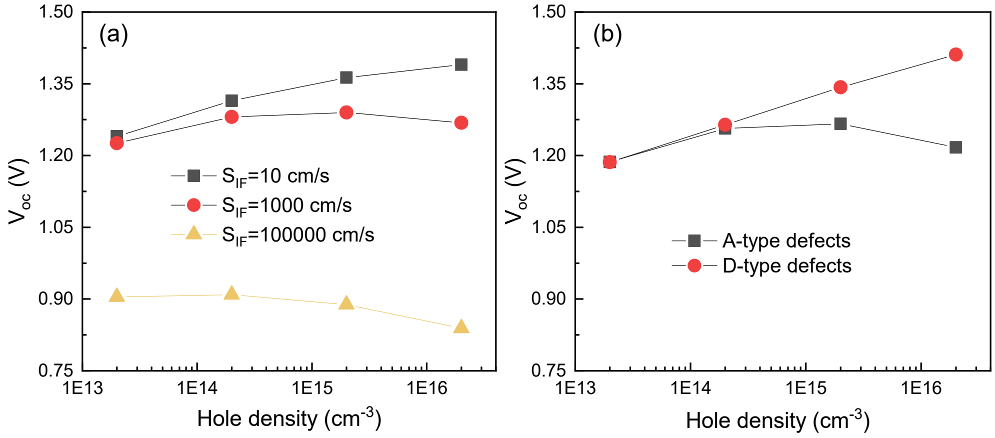

Figure 8: (**a**) The V_{oc} plots for Se solar cells with different hole densities, plotted against interfacial recombination velocity (S_{IF}). The interface defects were simulated as acceptor type, with a CBO of −0.2 eV. (**b**) The V_{oc} plots for solar cells with varying hole densities, comparing two types of interface defects. The S_{IF} was fixed at 1×10^5 cm/s, and the CBO was set to +0.2 eV.

3.3 Interface Passivated Strategy

Drawing on the analysis of interface property effects—including band alignment, defect density, and defect type—on Se solar cells, we establish the following design principles for emitter/Se absorber interfaces:

(1) Optimize band alignment: Select ETL materials with electron affinity equal to or slightly lower than that of Se. This configuration enhances absorber band bending and reduces hole concentration at the emitter/Se interface.

(2) Control interface defects: Either minimize defect density or introduce donor-type defects to suppress interfacial recombination.

Implementing Principle (1) requires ETL materials capable of forming small conduction band spikes—a significant challenge given Se's low electron affinity. To address this limitation, we propose a novel MIS-inspired passivation strategy featuring an atomic-scale dielectric interlayer (Fig. 9). This ultra-thin layer incorporates either positive charges (to enhance band bending, strengthen the built-in field, and promote tunneling), or hydrogen atoms (to passivate dangling bonds). Both approaches collectively mitigate interfacial recombination while facilitating electron transport across the interface.

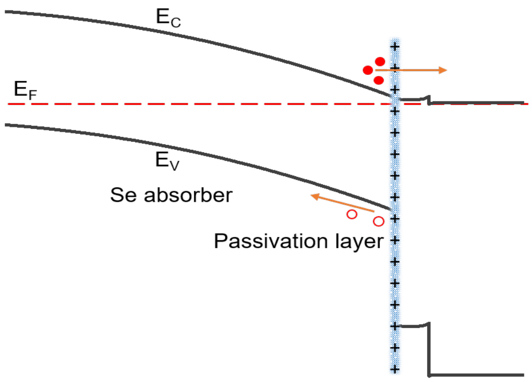

Figure 9: Schematic illustration of the interface-passivated Se solar cell structure proposed in this study.

4 Conclusion

Our numerical simulations underscore the critical role of interface properties in governing the performance of Se solar cells. The currently observed low open-circuit voltage in reported devices stems primarily from challenges in suppressing interfacial recombination. Theoretically, optimizing the emitter/Se interface through the selection of ETL materials to form a slight positive conduction band offset (or "spike") represents an effective strategy for achieving high-performance devices. However, Se's inherent low electron affinity typically results in an unfavorable conduction band cliff when paired with commonly employed ETLs. Consequently, identifying superior ETL materials capable of realizing the desired band alignment remains a key research objective. Furthermore, the well-established interface design principles for high-efficiency crystalline silicon heterojunction solar cells offer instructive guidance for Se cell interface engineering. Building on these insights, this study proposes a novel interface passivation strategy involving the incorporation of an ultra-thin passivation layer (e.g., a-SiN$_x$:H, a-Si:H) between the ETL and Se absorber. This approach is designed to mitigate interfacial recombination and enhance overall device performance. In summary, Se presents significant promise as a photovoltaic material, and substantial performance enhancement in Se solar cells is anticipated upon the effective suppression of interfacial recombination.

Acknowledgement: This work was supported by the Fundamental Research Funds of China West Normal University (No. 22kE035), the Innovation Team Funds of China West Normal University (KCXTD2024-4) and Leshan West Silicon Materials Photovoltaic New Energy Industry Technology Research Institute (2024GYKF6). The authors wish to thank the University of Ghent and the developers of SCAPS for making their software package publicly available free of charge.

Funding Statement: This research was supported by the Fundamental Research Funds of China West Normal University (No. 22kE035), the Innovation Team Funds of China West Normal University (KCXTD2024-4) and Leshan West Silicon Materials Photovoltaic New Energy Industry Technology Research Institute (2024GYKF6).

Author Contributions: The authors confirm contribution to the paper as follows: study conception and design: Fan He; data collection: Fan He and Jie Wang; analysis and interpretation of results: Fan He, Xu He and Yu Hu; draft manuscript preparation: Fan He. All authors reviewed the results and approved the final version of the manuscript.

Availability of Data and Materials: The data that support the findings of this study are available from the corresponding author（Fan He）upon reasonable request.

Ethics Approval: Not applicable

Conflicts of Interest: The authors declare no conflicts of interest to report regarding the present study.

References

1. Zhu M, Hao F, Ma L, Song T-B, Miller CE, Wasielewski MR, et al. Solution-processed air-stable mesoscopic selenium solar cells. ACS Energy Lett. 2016;1:469–73. https://doi.org/10.1021/acsenergylett.6b00249.
2. Todorov TK, Singh S, Bishop DM, Gunawan O, Lee YS, Gershon TS, et al. Ultrathin high band gap solar cells with improved efficiencies from the world's oldest photovoltaic material. Nat Commun. 2017;8:1–8. https://doi.org/10.1038/s41467-017-00582-9.
3. Hadar I, Song T, Ke W, Kanatzidis MG. Modern processing and insights on selenium solar cells: the world's first photovoltaic device. Adv Energy Mater. 2019;9:201802766. https://doi.org/10.1002/aenm.201802766.
4. Zhu M, Niu G, Tang J. Elemental Se: fundamentals and its optoelectronic applications. J Mater Chem C. 2019;7:2199–206. https://doi.org/10.1039/c8tc05873c.
5. Nakada T, Kunioka A. Polycrystalline thin-film TiO_2/Se solar cells. JPN J Appl Phys. 1985;24:L536. https://doi.org/10.1143/jjap.24.l536.
6. Youngman TH, Nielsen R, Crovetto A, Seger B, Hansen O, Chorkendorff I, et al. Semitransparent selenium solar cells as a top cell for tandem photovoltaics. Sol RRL. 2021; 5:2100111. https://doi.org/10.1002/solr.202100111.
7. Qian J, Jiang K, Huang J, Liu Q, Yang L, Song Y. A Selenium-based cathode for a high-voltage tandem photoelectrochemical solar cell. Angew Chem Int Ed Engl. 2012; 51:10351–4. https://doi.org/10.1002/anie.201204108.
8. Nielsen R, Hemmingsen TH, Bonczyk TG, Hansen O, Chorkendorff I, Vesborg PCK. Laser-annealing and solid-phase epitaxy of selenium thin-film solar cells. ACS Appl Energy Mater. 2023; 6:8849–56. https://doi.org/10.1021/acsaem.3c01464.
9. Nielsen R, Crovetto A, Assar A, Hansen O, Chorkendorff I, Vesborg PC. Monolithic selenium/silicon tandem solar cells. PRX Energy. 2024;3:013013. https://doi.org/10.1103/prxenergy.3.013013.
10. Nielsen R, Youngman TH, Moustafa H, Levcenco S, Hempel H, Crovetto A, et al. Origin of photovoltaic losses in selenium solar cells with open-circuit voltages approaching 1 V. J Mater Chem A. 2022;10:24199–207. https://doi.org/10.1039/d2ta07729a.
11. Pecunia V, Occhipinti LG, Hoye RLZ. Emerging Indoor photovoltaic technologies for sustainable internet of things. Adv Energy Mater. 2021;11:2100698. https://doi.org/10.1002/aenm.202100698.
12. Polyzoidis C, Rogdakis K, Kymakis E. Indoor perovskite photovoltaics for the internet of things—challenges and opportunities toward market uptake. Adv Energy Mater. 2021; 11:2101854. https://doi.org/10.1002/aenm.202101854.
13. Kavanagh SR, Nielsen RS, Hansen JL, Davidsen RS, Hansen O, Samli AE, et al. Intrinsic point defect tolerance in selenium for indoor and tandem photovoltaics. Energy Environ Sci. 2025; 18:4431–46. https://doi.org/10.1039/d4ee04647a.
14. Lu W, Feng M, Li Z, Yan B, Wang S, Wen X, et al. Ordering one-dimensional chains enables efficient selenium photovoltaics. Joule. 2024;8:1430–42. https://doi.org/10.1016/j.joule.2024.02.024.
15. Liu Q, Wang X, Li Z, Lu W, Wen X, An X, et al. Standing 1D Chains enable efficient wide-bandgap selenium solar cells. Adv Mater. 2024;37:e2410835. https://doi.org/10.1002/adma.202410835.
16. An X, Li Z, Wang X, Lu W, Wen X, Feng M, et al. Photovoltaic absorber "Glues" for efficient bifacial selenium photovoltaics. Angew Chem Int Ed Engl. 2025; 64:e202505297. https://doi.org/10.1002/anie.202505297.
17. Degrave S, Burgelman M, Nollet P. Modelling of polycrystalline thin film solar cells: new features in SCAPS version 2.3. In: Proceedings of the 3rd World Conference on Photovoltaic Energy Conversion; 2003 May 11–18; Osaka, Japan.
18. Gloeckler M, Fahrenbruch AL, Sites JR. Numerical modeling of CIGS and CdTe solar cells: setting the baseline. In: Proceedings of the 3rd World Conference of Photovoltaic Energy Conversion; 2003 May 11–18; Osaka, Japan.
19. Feng Y, Wang T, Yu M, Huang J, Li W, Hao X, et al. Coevaporated Cd_{1-x}MgxTe thin films for CdTe solar cells. Renew Energy. 2020;145:13–20. https://doi.org/10.1016/j.renene.2019.05.139.
20. Wilhelm H, Schock H-W, Scheer R. Interface recombination in heterojunction solar cells: influence of buffer layer thickness. J Appl Phys. 2011;109:084514. https://doi.org/10.1063/1.3554409.
21. Song T, Kanevce A, Sites JR. Emitter/absorber interface of CdTe solar cells. J Appl Phys. 2016;119:233104. https://doi.org/10.1063/1.4953820.
22. Nielsen R, Youngman TH, Crovetto A, Hansen O, Chorkendorff I, Vesborg PCK. Selenium Thin-film solar cells with cadmium sulfide as a heterojunction partner. ACS Appl Energy Mater. 2021;4:10697–702. https://doi.org/10.1021/acsaem.1c01700.
23. Thomas L, Don C, Major J. An investigation into the optimal device design for selenium solar cells. Energy Rep. 2022;8:14–22. https://doi.org/10.1016/j.egyr.2022.05.045.